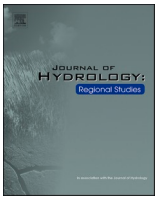
Journal of Hydrology: Regional Studies 60 (2025) 102508



Contents lists available at ScienceDirect

Journal of Hydrology: Regional Studies

journal homepage: www.elsevier.com/locate/ejrh



Tree-ring based May-June streamflow reconstruction of Zemu River in the Eastern Himalaya

Nazimul Islam [a,b,*], Torsten Vennemann [a], Ulf Büntgen [b,c,d], Paul J. Krusic [b,e], Santosh K. Shah [f], Stuart N. Lane [a]

[a] Institute of Earth Surface Dynamics (IDYST), University of Lausanne, Switzerland
[b] Department of Geography, University of Cambridge, United Kingdom
[c] Department of Geography, Faculty of Science, Masaryk University, Brno, Czech Republic
[d] Global Change Research Institute of the Czech Academy of Sciences, Brno, Czech Republic
[e] Department of History, Stockholm University, Stockholm, Sweden
[f] Birbal Sahni Institute of Palaeosciences (BSIP), Lucknow, India

ARTICLE INFO

Keywords:
Tree rings
Streamflow reconstruction
Zemu River
Eastern Himalaya

ABSTRACT

Study region: Zemu River, Upper Teesta River Basin, Eastern Himalaya
Study focus: In this study, a tree-ring chronology of Abies densa was used as a proxy to reconstruct a century-long May-June streamflow of the Zemu River. The reconstruction was carried out based on a scaling approach which explained 35 % of variance in observed streamflow and was varified by comparing with other regional reconstructions. Moving windowed Pearson correlation was performed to reveal the temporal influence of major climate forcings (e.g., ENSO) with the streamflow of Zemu River.
New hydrological insights for the region: Our study identified a strong negative relationship between tree-growth and observed May-June streamflow in the glacier-fed Zemu River. This counterintuitive, inverse relationship is likely due to the contribution of additional meltwater when conditions are dry and insulation over the glacier is high. The reconstructed streamflow record reveals several high- and low-flow periods above and below the mean value (+/- 1σ) and identifies 30 high-flow years and 33 low-flow years, including some historically recorded floods in 1927, 1968, 1980, 1982 and 1998, and of severe droughts in 1951, 1976 and 2017. Most recently, a positive association between reconstructed streamflow and the ENSO has become apparent, which we attribute to reduced penetration of the Indian Summer Monsoon during ENSO years, which reduces precipitation but maintains for longer warmer and drier conditions that allow glacier melt.

1. Introduction

The impacts of climate change are greater in high-altitude mountain environments than in lowlands (Kraaijenbrink et al., 2017; Pepin et al., 2022; Rangwala and Miller, 2012; Schmeller et al., 2022). This is because rapid warming leads to feedback associated with albedo, cloud cover, water vapour, aerosols, blackbody emissions etc. that amplify the warming signal (Pepin et al., 2015). In the cryosphere, snow and glaciers are particularly sensitive to climate change (Carrer et al., 2023; Roe et al., 2017). In recent decades, High

* Correspondence to: Institute of Earth Surface Dynamics (IDYST), University of Lausanne, Lausanne CH-1015, Switzerland.
E-mail address: nazimul.islam@unil.ch (N. Islam).

https://doi.org/10.1016/j.ejrh.2025.102508
Received 25 January 2025; Received in revised form 23 May 2025; Accepted 4 June 2025
2214-5818/© 2025 The Author(s). Published by Elsevier B.V. This is an open access article under the CC BY license (http://creativecommons.org/licenses/by/4.0/).

Mountain Asia (HMA) has been at the centre of global climate change research because of a growing concern that warmer climate periods will reduce freshwater availability and increase the frequency and magnitude of natural hazards. Glaciers and snow cover supply freshwater to more than 1.5 billion people in the major river basins across the HMA (Immerzeel et al., 2020, 2010; Li et al., 2021). Projected climate change is a major issue (Dimri et al., 2018; Rani et al., 2022; Wijngaard et al., 2018), because the Himalayan 'water towers' (Immerzeel et al., 2020, 2010; Viviroli et al., 2007) are continuously losing mass even if the extent and rate is not always clear (Kääb et al., 2012; Lee et al., 2021; Zhang et al., 2023). Many of these river basins are also experiencing decreasing water availability and increasing magnitude and frequency of natural hazards including outburst floods, and droughts (Katel et al., 2015; Kattel et al., 2023). A recent study by Shrestha et al. (2023) reported a total of 697 glacial lake outburst floods (GLOFs) between 1833 and 2022 causing approximately 7000 fatalities in the HMA. It is estimated that 9.3 million people are exposed to GLOF risk from over 2000 glacial lakes across the HMA (Taylor et al., 2023).

Despite the risk of extremely severe climate impacts across the HMA, there are relatively few instrumental records, the longest of which begins in the early twentieth century (Jaffrés, 2019). The lack of long-term instrumental records makes it particularly difficult to separate anthropogenic climate-related change from natural variability and therefore understand how snow- and glacier-melt changes have historically impacted streamflow (Kayastha and Kayastha, 2019). To fill this knowledge gap, several studies have reconstructed streamflow in Himalayan rivers using proxy records in tree rings (see review in Islam et al., 2024). The majority of tree-ring based streamflow reconstructions are available for Western Himalayan rivers and only a few streamflow records are available for rivers in the Eastern Himalaya. Some reconstructions are not up to date as they are more than one or two decades old. For instance, there are streamflow reconstructions covering the period 1309–2008 for the Brahmaputra River (Rao et al., 2020), 1790–1994 for the Lachen River (Shah et al., 2014), 1846–1999 for the Lohit River (Shah et al., 2019), and 1775–1996 for the Zemu River (Shekhar and Bhattacharyya, 2015). There are also questions of reliability concerning some of these reconstructions. For instance, the Zemu River analysis in Shekhar and Bhattacharyya (2015) uses instrumental streamflow data from 1976 to 1996 that are different to the official data we have obtained for the same station. Furthermore, they validated their reconstruction based on a split sample method instead of applying the leave-one-out method which is more widely used for short duration datasets (Michaelsen, 1987).

The need for such long historical records is reinforced by the growing sense that in these regions natural variability is not

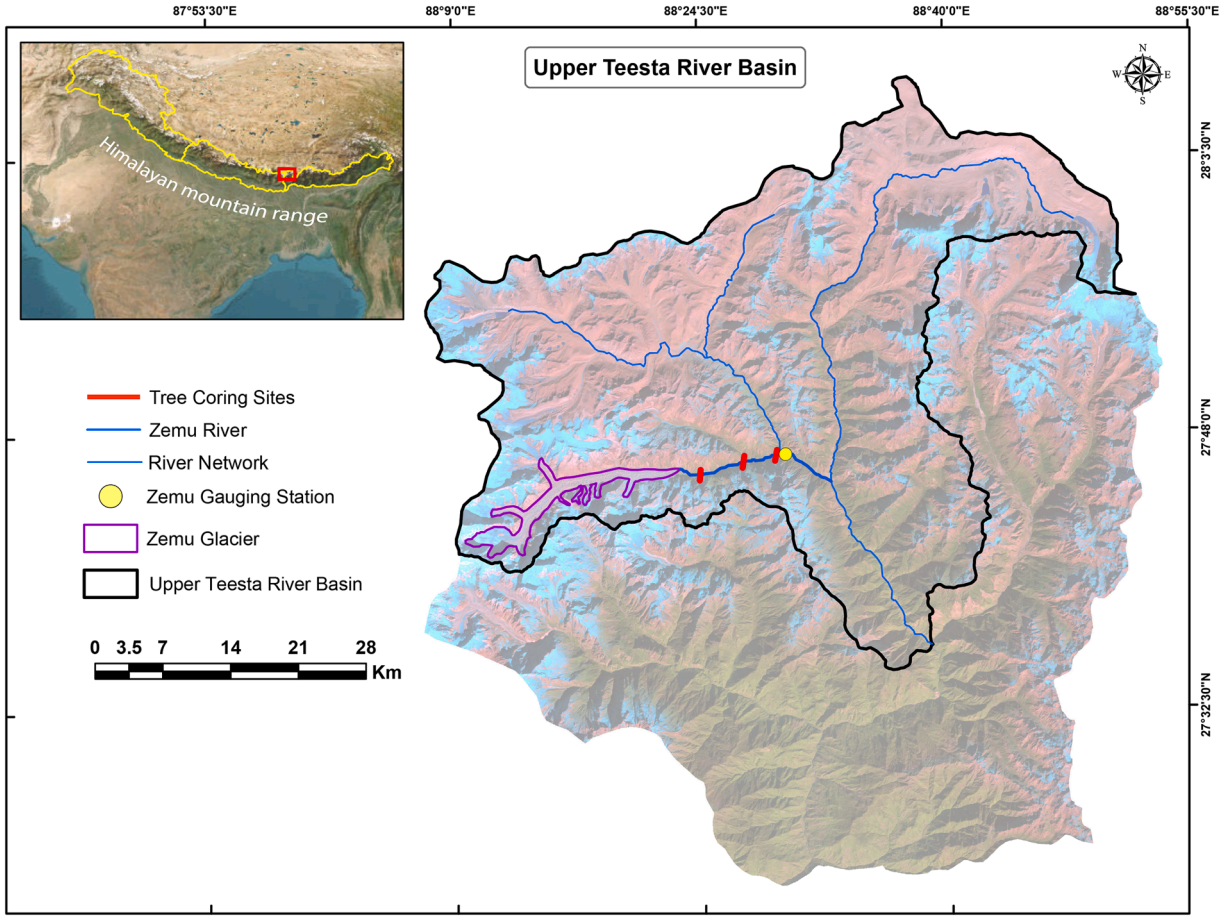


Fig. 1. Locations of the tree-ring sampling sites and hydrological station along the Zemu River in the Upper Teesta River Basin, North Sikkim, Eastern Himalaya.

statistically stationary due to climate forcing. Studies have shown that streamflow variability in Himalayan rivers is affected by global climate phenomenon such as the El Niño-Southern Oscillation (ENSO) in particular. ENSO brings dry and wet conditions to this region and is considered a driver of the South Asian Summer Monsoon (Gaire et al., 2024, 2019, 2017; Yadav, 2011; Yadav et al., 2014), causing erratic precipitation patterns in the mountains of northeastern India (Shah et al., 2019, 2014). The relationship of ENSO with streamflow in the Himalayan rivers has not been explicitly discussed in existing studies. Thus, the aims of this study are (1) to reconstruct the pre-monsoon streamflow of the Zemu River, a river in North Sikkim, Eastern Himalaya using a variance stabilized ensemble tree-ring chronology of *Abies densa*, and (2) to use this reconstruction to quantify long-term hydrological changes in this river by identifying what linkages exist between streamflow variability and large-scale climate forcing.

2. Materials and methods

2.1. Study area

The Upper Teesta River Basin (2080 km^2) is located in the northern part of the Indian state of Sikkim (27°7′15″N to 27°34′10″N and 88°7′30″E to 88°51′32″E) at an elevation of 1500 m to 8000 m above mean sea level (a.m.s.l.). Many glaciers and glacial lakes are found in the Upper Teesta basin (Islam and Patel, 2021). The Zemu River is a right bank tributary of the Lachen River that originates from the Zemu Glacier (~42 km^2), the second largest glacier in the Himalaya and the largest in the Eastern Himalaya (Debnath et al., 2018; Shukla et al., 2018). It is one of seventeen watersheds of the Teesta River. The Zemu catchment is an important headwater catchment in terms of freshwater contribution (Fig. 1). The catchment area of the Zemu River is ~340 km^2 and is highly glacierised. In the moist-temperate to sub-alpine forested catchment zones the most dominated tree species is Bhutan fir (*Abies densa)*.

2.2. Tree ring data and chronology development

In May 2022, tree ring samples from 15 *A. densa* trees, the dominant vegetation cover, were collected. Three sites at 4 km intervals along the river were selected at elevations ranging from 3200 m to 3700 m a.m.s.l. The topography and local climatic conditions show homogeneity in all three sites making them comparable. At each site, trees both close and distal to the river were sampled. The trees close to the river were located at the edge of the Zemu river banks and considered as proximal trees. Trees located away from the Zemu river were considered as distal trees. The geographical locations (XY-coordinates, elevations and distances of the trees from the Zemu River) are provided in Supplementary file S1. Two cores were taken from each tree using increment borers. All samples were stored in air-limiting handmade paper straws. Upon return to the laboratory, cores were individually fixed in wooden mounts, naturally air-dried for a few days and then sanded using different grits of sandpapers (e.g., 180, 400 and 600 grits). The tree rings were distinct with clearly visible ring boundaries as well as the intra-annual transition from earlywood to latewood. In total, 30 cores from 15 undisturbed *A. densa* trees along the Zemu river were prepared for this study (Table 1).

The smooth, polished, cross-sectional surfaces of the samples were then scanned using a high-resolution, automated, image capture system called Skippy© (Gärtner et al., 2024). After scanning, each ring from every core was measured to ±1/1000 mm precision using the CooRecorder and CDendro 9.6 software suite (Maxwell and Larsson, 2021). Each core's measurement accuracy and dating precision was evaluated using the COFECHA program (Grissino-Mayer, 2001; Holmes, 1983). The dating of all samples was deemed satisfactory after correction of errors that occurred due to the presence of false and locally absent rings detected by COFECHA. Initially, two chronologies were produced, one from the trees proximal to the river and another from trees distal to the river. Program ARSTAN (Cook, 1985; Cook et al., 2017; Cook and Holmes, 1996) was used to check the degree of coherence between the two site chronologies (Fig. 2a). Our results show that the proximal and distal chronologies were highly correlated, suggesting our criteria for selecting individual tree based on distance from the river had no significant influence on the common growth history at our study area. This was further confirmed by a student's *t*-test with no significant inter-site tree growth differences (at $p = 0.05$). Therefore, all site data were combined and used to develop a single Zemu River, *A. densa* chronology. The tree ring standardization technique used in this study employed multiple curve-fitting methods (Fig. 2b). Standardization is a technique used to eliminate age related growth trends due to biological maturation and physical geometry thereby transforming raw ring-width measurement values into dimensionless indices (Douglass, 1919; Fritts, 1976, 1971; Schulman, 1956). Different standardization techniques including the cubic spline (Cook and Peters, 1981), regional curve standardization (Briffa et al., 1992; Helama et al., 2017; Melvin et al., 2007), multiple regional curve

Table 1
Quantitative assessment of the ensemble tree-ring chronology in the Zemu River catchment.

• No. of cores and trees	30/15
• Chronology length	182 years
• Chronology period	1840–2021
• Mean sensitivity	0.20
• Inter-series correlation	0.52
• Mean growth	1.40 ± 0.45 mm
• Standard deviation (σ)	0.42
• Mean Rbar ($\bar{r}$)	0.32
• EPS	> 0.85 (1849–2021)

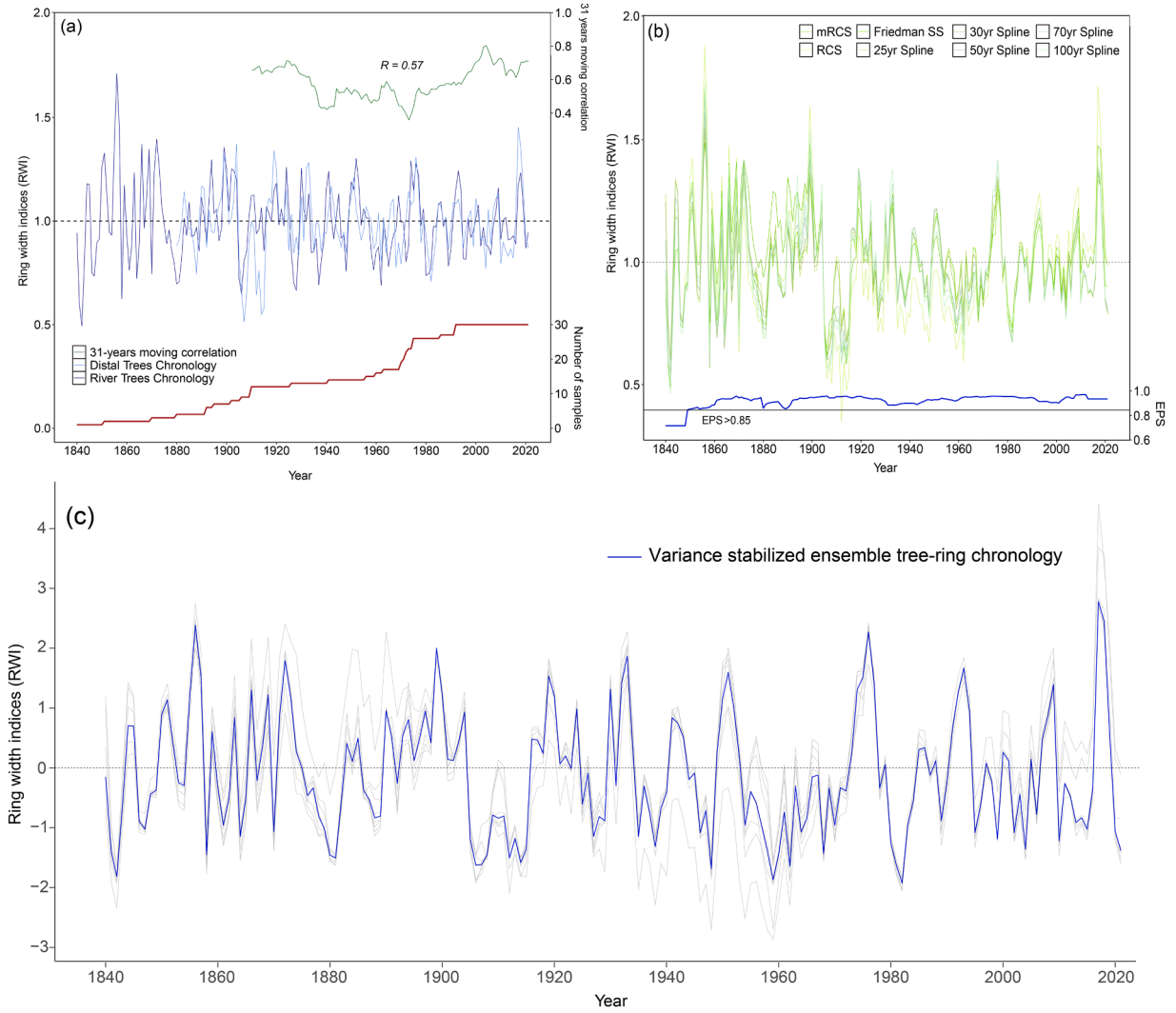


Fig. 2. RWI chronology of proximal and distal trees to the Zemu River together with the number of samples used (a), RWI chronology of Zemu River using eight different standardization techniques along with the EPS scores (b), and the final variance stabilized ensemble RWI chronology (denoted in blue) used in this study (c).

standardization (Briffa and Melvin, 2011), and Friedman's super smoother (FSS; Friedman, 1984) were applied to remove presumed non-climatic, low-frequency variance. The cubic spline detrending applies a flexible, smooth spline curve algorithm (Reinsch, 1971, 1967) to remove non-climatic signals (Bussberg et al., 2020). This technique is suitable for preserving high-frequency (e.g., year-to-year) variations while accounting for age related growth and allows control over the stiffness of the curve retaining desired climate signals. In this study, the cubic spline was used at both higher and lower smoothing flexibilities (e.g., 25-, 30-, 50-, 70- and 100-years) to fit multiple smoothing curves for removing biological growth trends. Regional curve standardization (RCS) method can retain more long-term climate, low-frequency estimates of climate trends information as it allows for a larger extent of over- and underestimation of tree growth to occur (Cook et al., 1995; Helama et al., 2017). This detrending technique combines growth data from many trees to establish an average growth curve, which is then used to detrend individual tree-ring growth series and is considered as an effective method to capture long-term climate variability across multiple samples. Multiple regional curve standardization (mRCS) is an advanced modification of the RCS detrending technique. The mRCS involves in partitioning of the individual tree's data to a number of age/ growth classes (e.g., 6, 9 or 12) based on specific growth-related characteristics (e.g., mean or median growth rates, site conditions, tree species) in a collection, followed by applying individual regional growth curves to each group. The mRCS detrending method allows for the condition that not all trees grow at the same rate relative to their age and is assumed to better preservation of low frequency variability with lower uncertainty which may not be possible by simply applying the cubic spline or simple RCS. Unlike other standardization methods, the FSS is an adaptive smoothing algorithm induced by Friedman (1984) for which the smoothing span is based on time-localised data characteristics, making it appropriate for capturing complex patterns in time-series data. The FSS allows removal of high frequency non-climatic noise due to forest stand dynamics, as well as biological age trend, and

still preserve low-frequency climatic signals (Friedman, 1984; Matheus, 2014). By applying these different standardization techniques, eight unique chronologies were produced in this study. Variance stabilization was applied to all eight chronologies to address any residual non-climatic noise in the chronologies. Variance stabilization methods reduce bias by eliminating the variance fluctuations due to changing sample size, particularly further back in time when there may be fewer cores available to construct the chronology (Frank et al., 2006; Osborn et al., 1997). Combining these techniques together to develop a single ensemble tree-ring chronology (Fig. 2c) is valuable, as it removes both undesirable low- and high-frequency age and forest dynamical growth trends, omnipresent in the highly complex hydrological and geomorphological conditions common to Himalayan River basins.

A suite of chronology-related statistics, including the inter-series correlation, mean sensitivity, expressed population signal (EPS) etc. were calculated using the dplR package (Bunn, 2010, 2008) in the R-programming environment to verify the common signal quality and dating precision. The inter-series correlation shows a high degree of agreement in growth patterns between individual trees and the average site chronology. The mean sensitivity quantifies the year-to-year variability in tree-ring width and the value ranges between 0 and 1. Tree-ring series with a mean sensitivity of 0.2 and above are considered to be sensitive enough to environmental information and thus can be used for climatic reconstruction (García-López et al., 2022; Speer, 2010). The EPS is a tool to measure the common variability in the chronology with regard to sample depth (Speer, 2010). An EPS value of 0.85 is considered the standard threshold above which a chronology is considered to contain a high degree of shared variance over time and thereby suitable for climatic reconstruction (Wigley et al., 1984). Chronologies with periods of low EPS values indicate they may not necessarily have enough useful common signal for our streamflow reconstruction (Buras, 2017). We further calculated the running Rbar ($\bar{r}$) to measure common signals between tree-ring series with a 20-year window and a 19-year overlap (Wigley et al., 1984; Wilson et al., 2017).

2.3. Meteorological and hydrological data

The Upper Teesta River Basin is a poorly-gauged glacierized basin and most of the basin is highly inaccessible due to extremely steep terrain. Thus, there are no meteorological stations in this region that can provide long-term climate records. The nearest Indian Meteorological Department (IMD) station is located in Gangtok, ~150 km from the study site. Therefore, we collected monthly

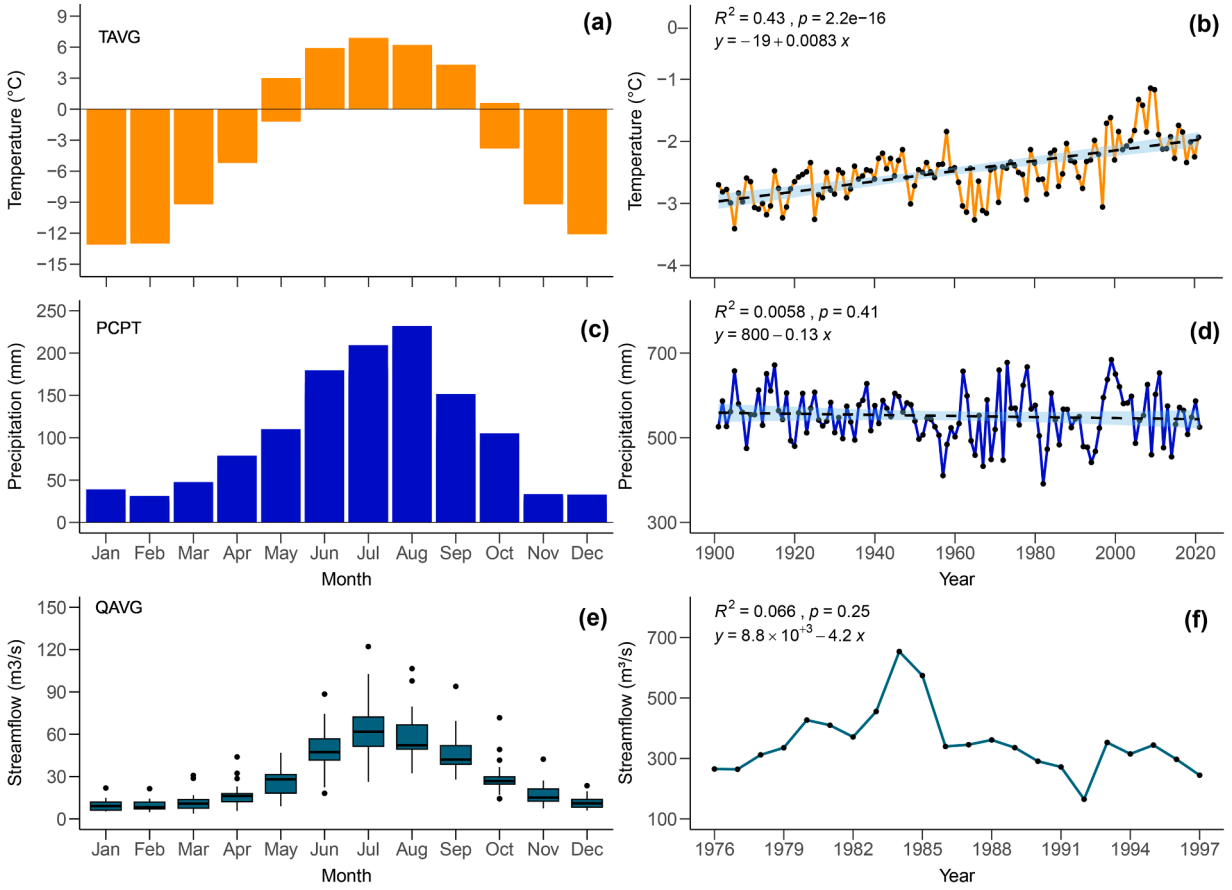


Fig. 3. Monthly mean and annual mean temperature; TAVG (a, b) and precipitation; PCPT (c, d) data at the study site (Source: CRU) and streamflow; QAVG (e, f) data of the Zemu River (Source: NHPC), Sikkim, Eastern Himalaya. The dashed lines denote trends in the annual hydroclimatic data. The blue band indicates 95 % confidence levels.

average temperature and precipitation data from the Climate Research Unit (CRU; Harris et al., 2020) time series (TS 4.07) for 27.75° N and 88.25° E. The data covers the years 1901–2021 (http://climexp.knmi.nl). Besides temperature and precipitation, we also collected global climate forcing data, notably the ENSO index (Ropelewski and Jones, 1987) from the CRU dataset available at the University of East Anglia (https://crudata.uea.ac.uk/cru/data/pci.htm).

The average temperature range is between −13.1 °C in winter (e.g., in January) and 6.9 °C in summer (e.g., in July) with an annual average temperature of −2.5 °C during the analysis period between 1901 and 2021 (Fig. 3a). The annual average temperature time-series (Fig. 3b) shows a significant linear trend of increasing temperature (R^2=*0.43*, $p < 0.01$) and this trend is stronger from 1960 onwards. The annual average precipitation in this region is 551 mm and the lowest and highest precipitation is recorded in winter and in summer respectively (Fig. 3c). Due to the influence of the Indian Summer Monsoon (ISM), 75 % of the annual average precipitation occurs in summer between June to September.

Streamflow data for the Zemu River recorded at the Zemu gauge station (27°46 50 N and 88°29 28 E) were obtained from the National Hydroelectric Power Corporation (NHPC). The streamflow data are available only for the period from 1976 to 1997 as this gauge station is no longer in operation. The Zemu catchment is relatively inaccessible and not particularly impacted by humans. Thus, the observed variations in streamflow are likely to reflect natural hydrological variability under changing climate. Fig. 2 shows that between 1976 and 1997, the Zemu River had an annual average streamflow of 351.3 m^3 /s. The recorded maximum and minimum

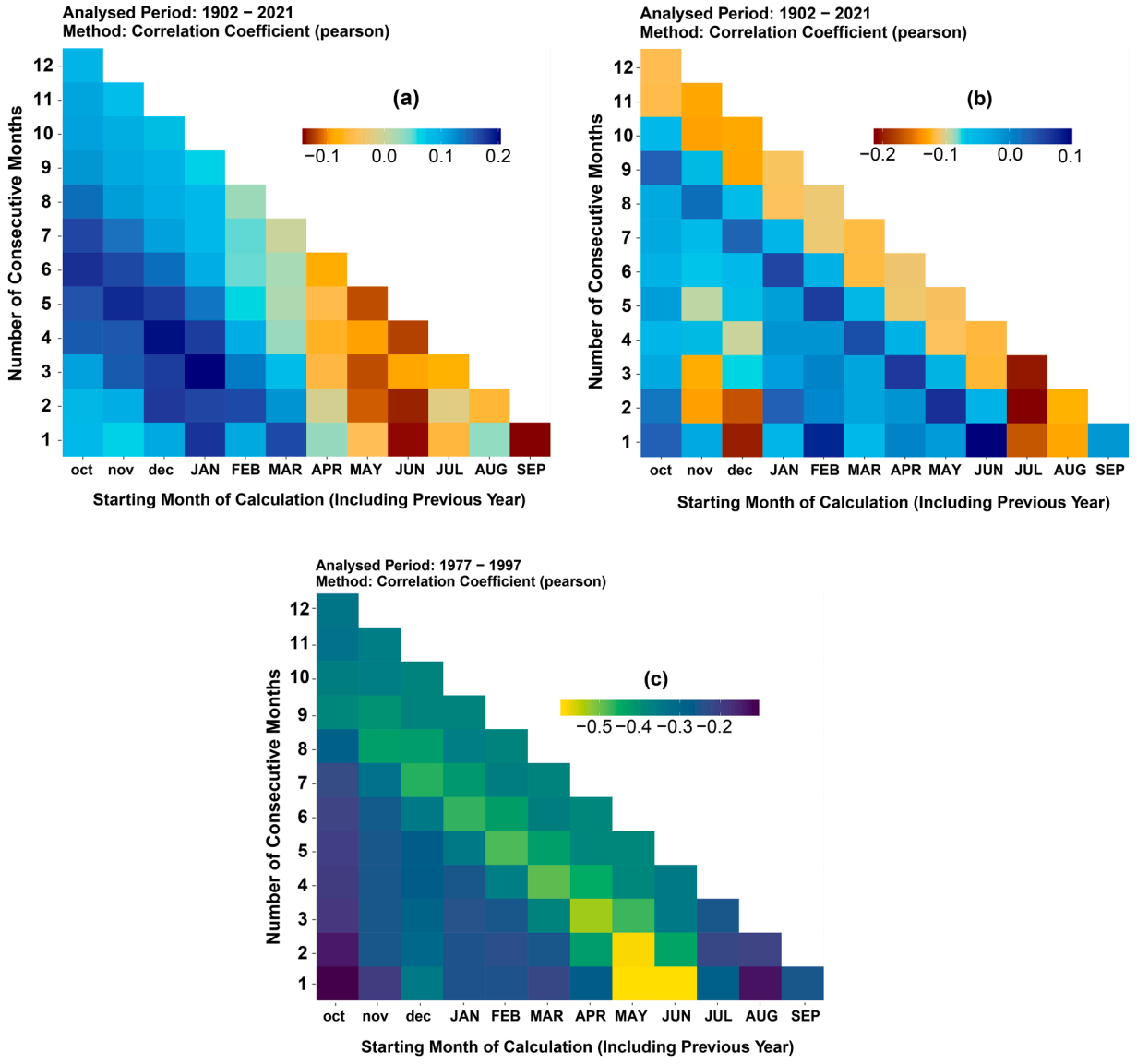


Fig. 4. Heatmap for the temporal relationships between the ensemble RWI chronology and temperature (a), precipitation (b) and streamflow (c). Correlation values are shown in the coloured scale bar. Analysis period for climate data (e.g., temperature and precipitation) is 1902–2021, and for hydrological data (e.g., streamflow) is 1977–1997.

flows were 653.5 m^3 /s in 1984 and 165.0 m^3 /s in 1992 respectively. The Box-and-Whisker plot in Fig. 3e shows that the Zemu River reaches its maximum streamflow during the summer months from June to September, i.e., 66.8 % of the average annual streamflow. This is due to temperature-induced snow and glacier melt and as well as ISM influence.

2.4. Growth-hydroclimate response analysis

Monthly and seasonal relationships between tree growth and climatic parameters notably temperature, precipitation and streamflow were derived by performing Pearson's correlation analysis. The correlation coefficients are calculated using the "monthly response()" function in the dendroToolsR package (Jevšenak and Levanič, 2018). For computing the correlation coefficients, we defined the hydroclimatic year as starting in October of the previous year and ending in September of the current year, and the number of months for which the correlation is calculated, starting from 1-month to 12-month windows, shown in the x- and y-axes respectively in Fig. 4. The significance level of a correlation was assessed at $p < 0.05$ (95 %) for climate data (e.g., temperature and precipitation for the period 1901–2021) and for the hydrological data (e.g., streamflow) for the period 1976–1997. Acress both periods, the highest correlations found between tree growth and Zemu river streamflow, were those for the months May and June.

2.5. Streamflow reconstruction

A scaling approach (Büntgen et al., 2017) was used to reconstruct streamflow using the following two-step formula (Eq. 1 & 2).

$$RWI = X * \sigma Q / \sigma X \tag{1}$$

$$Streamflow = RWI - \quad \overline{RWI} + \overline{Q} \tag{2}$$

where RWI is the variance stabilized ensemble RWI chronology, X is the variance stabilized median^{-1} time series, Q is the observed May-June average streamflow of each year, and $\sigma Q, \sigma X$ are the standard deviations in observed streamflow and the variance stabilized median^{-1} time series respectively.

The uncertainty in the reconstructed streamflow record was calculated following Büntgen et al. (2017); (Eq. 3 & 4)

$$Minimum\ uncertainty = RWI - RWI_{error} - SS_{error} - \sqrt{Q_{RMSE} \quad / \quad Q_n} \tag{3}$$

$$Maximum\ uncertainty = RWI + RWI_{error} + SS_{error} + \sqrt{Q_{RMSE} \quad / \quad Q_n} \tag{4}$$

where, RWI_{error} is the difference between the variance stabilized minimum^{-1} and maximum^{-1} time series, SS_{error} is the sample size error which is denoted as 1 minus the sample size of each year, and Q_{RMSE}, Q_n are the root mean square error and total number of years in the observed streamflow.

Since the observed streamflow record for the Zemu gauging station is only 22 years long (1976–1997), any formal validation of the reconstruction could not be performed. The estimated streamflow records of this period (1976–1997) were validated using a leave-one-out cross validation test (Michaelsen, 1987). The correlation coefficient (r), coefficient of determination (r^2), and reduction error (RE) were used to evaluate the reliability of the reconstruction (Table 2). A robustification method was applied to the reconstructed May-June streamflow during the period of available observed streamflow (1976–1997). Data robustification is the process which aims to mitigate the effects of data errors, missing data, and outliers to achieve a better model fit (Huber, 1981; Rousseeuw and Leroy, 1987). Here, it served to reduce the effects of outliers on the reconstruction and improve the relationship between observed and reconstructed streamflow record. Additional evaluation was possible by comparing our reconstruction with other streamflow reconstructions at neighbouring sites in the Himalaya. To investigate high and low streamflow years in all reconstructed time-series, we defined high streamflow values as ones greater than the mean $+1\sigma$ and low streamflow as ones smaller than the mean -1σ. A similar method has also been used in other studies (Gou et al., 2010; Shekhar and Bhattacharyya, 2015; Zhao et al., 2022). We applied an 11-year low-pass filter to smooth the reconstruction and show the range of low frequency variation in the reconstructed streamflow record. To tease out the relationship between reconstructed Zemu streamflow and various climate parameters (i.e., temperature, precipitation and ENSO) over a longer timescale , we performed windowed Pearson correlation in which the sign of the correlation depends on the window size and year.

Table 2
Leave-one-out cross validation test results for the May-June streamflow reconstruction.

• Correlation coefficient (r),	-0.83
• Coefficient of determination (r^2),	0.69
• Reduction error (RE)	0.63
• Product mean test (PMT),	3.15
• F test (F),	45.18
• Sign test (ST)	$19^+/3^-$

3. Results

3.1. Tree ring chronology and streamflow response

The variance stabilized ensemble RWI chronology is 182 years long, from 1840 to 2021, composed of information from 30 *A. densa* tree cores from three sites along the Zemu River. The inter-series correlation between each core's ring-width measurements and the mean of all series (-1) is 0.52, and the mean sensitivity is 0.20 (Table 1). The mean annual tree growth in this region is 1.42 ± 0.42 mm. The mean EPS is above 0.85 and the mean Rbar is 0.32. These overall chronology statistics provide evidence that the ensemble method of chronology construction captured a strong degree of common signal amongst the individual series.

The heatmaps in Fig. 4 shows the correlation between variance stabilized ensemble ring-width index chronology and temperature (a), precipitation (b) over the period 1902–2021, and streamflow (c) from 1977 to 1997. The correlations start in the previous year's October and end in September of the current year, that is the span a hydrological year, appropriate for a glacial catchment where most summer melt has ended by late September. RWI is positively correlated with temperature from October to March, but negatively with temperature from April to September. Precipitation is positively correlated with RWI between October and June but negatively correlated between July and August. The RWI correlations with temperature and precipitation are weak. The highest positive correlation between RWI and temperature is from January to March ($r = 0.20$, $p < 0.01$) and the lowest negative correlation with precipitation from July to August ($r = -0.21$, $p < 0.01$). Unlike temperature and precipitation, Zemu catchment tree-ring growth appears to capture a strong streamflow signal. A negative correlation is observed for all months, with the maximum negative correlation for May to June ($r = -0.59$, $p < 0.01$). Therefore, we considered the implications of this negative correlation (Fig. 4c) and reconstruct Zemu River streamflow for the period of May to June. This is a period of significant scientific interest as it is the transition period for the south-west Indian monsoon.

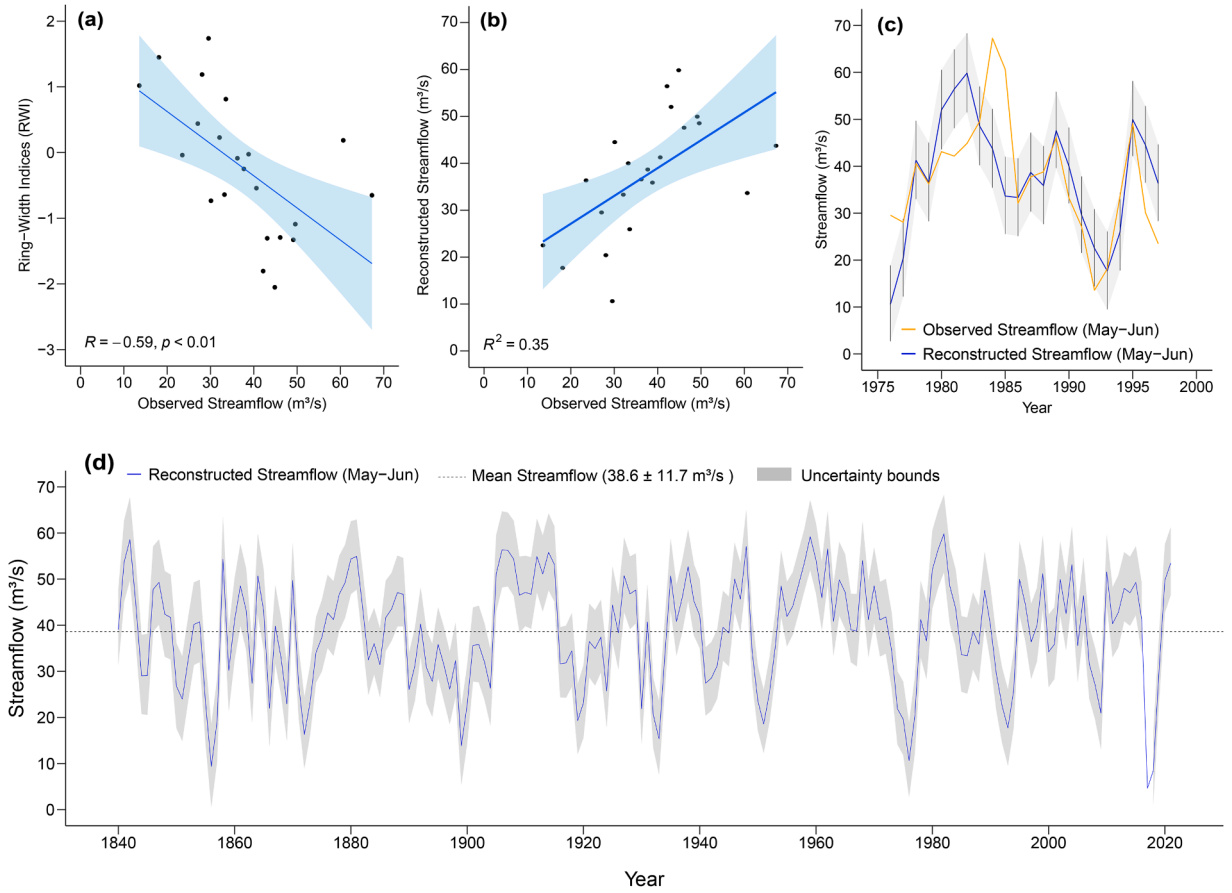


Fig. 5. Scatter plot of the RWI chronology and observed streamflow (a), observed and reconstructed May-June Zemu River streamflow (b) with their linear relationships highlighted during the period of 1976–1997. Comparison between the observed and reconstructed May-June streamflow from 1976 to 1997 (c), and 182-years long May-June streamflow reconstruction for 1840–2021 (d). The blue line denotes the reconstructed streamflow with uncertainties (i.e., the maximum and minimum errors in the reconstructions calculated based on RWI chronology errors, sample size errors and the root mean square errors) shown in grey shading.

3.2. Variability in reconstructed streamflow records

Based on the strength of the relationship ($r = -0.59$, $p < 0.01$) between tree growth and May-June Zemu River flow, our reconstruction accounts for 35% (R^2=0.35) of the observed variance from 1976 to 1997 (Fig. 5a-b). The leave-one-out (Michaelsen, 1987) results show that the variance captured by the reconstructed streamflow is 69 % (R^2=0.69) and has been used to validate our streamflow reconstruction record (Table 2). The reconstruction captured both high and low-frequency streamflow variability and agrees well with the observed streamflow record (Fig. 5c). Our reconstruction of Zemu river May-June streamflow extends from 1840 to 2021 for a total of 182 years. The mean reconstructed streamflow during this period is 38.6 ± 11.7 m^3 /s (Fig. 5d). Several low-flow and high-flow years are identified in this century-long streamflow reconstruction, but no significant long-term trend ($p > 0.05$) is present in the record, as confirmed by the Mann-Kendall test.(Fig. 6)

We found several distinctive periods of prolonged high streamflow, notably 1876–1882, 1905–1915, 1957–1962 1980–1983, and 2020–2021 and low streamflow, notably 1851–1857, 1866–1875, 1890–1904, 1916–1924, 1932–1934, 1973–1979, and 2017–2019. Over the span of 182 years of streamflow reconstruction, we have identified 33 low streamflow years i.e., 18.1 % of the total reconstruction length (values below mean − 1σ) and 30 high streamflow years i.e., 16.5 % of the total reconstruction length (values above mean + 1σ; Table 3). The years with the lowest streamflow are 2017 (4.6 m^3/s) and 2018 (8.5 m^3/s), which are 88.1 % and 78.0 % lower than mean reconstructed streamflow (38.6 ± 11.7 m^3/s) respectively. The highest streamflow year is 1982 (59.8 m^3/s), i.e., 55.0 % higher than the mean.

Fig. 7 shows the distribution of below-average, above-average, low-flow and high-flow years in four different 50-year window periods (e.g., 1840–1890, 1891–1940, 1941–1990, and 1991–2021). 22 below-average (12.1 %), 29 above average (16.0 %), and 10 low- and 10 high-flow years were identified between 1840 and 1890. For 1891–1940, the number of below-average flow years increased to 23 (14.8 %), and above-average flow years decreased to 23 (12.6 %), whereas the number of low- and high-flow years are 10 (5.5 %) and 7 (3.9 %). For 1941–1990, the number of below-average flow years decreased to 18 (9.9 %), and the number of above-average flow years increased to 31 (17.0 %), while 7 low- and 9 high-flow years were identified. In the recent period between 1991 and 2021, both the number of below-average (14) and above-average flow (17) years, as well as low-flow (6) and high-flow (4) years were fewer.

3.3. Relationship between the reconstructed streamflow and hydroclimatic variabilities

The correlations between reconstructed streamflow and hydroclimatic parameters shown in Fig. 8a may hide variability associated with different timescales. The results of windowed Pearson correlations (Fig. 8b) suggest time-dependent and scale-dependent responses. For instance, the correlation between streamflow and temperature tends to be positive at the beginning of the observation period and over short time-periods, for 1900–1910, in the 1930s, 1970s, and from the late 1980s. For time-scales over 20 years and longer, the correlations become generally positive over time, and at the scale of the entire dataset the association with temperature is positive. Precipitation shows a positive correlation with streamflow over shorter time-scales in the 1920s, 1950s and 1990s, however since 2000 this relationship has become negative. The relationship between ENSO and reconstructed streamflow is negative over short time-scales at the beginning of the analysis period until the late 1980s, with some periods of positive correlation in the 1920s, 1940s, and 1960s. However, from the late 1980s onwards a positive relationship is observed and, as with temperature, this is seen over progressively longer time-scales further back into the 20th century.

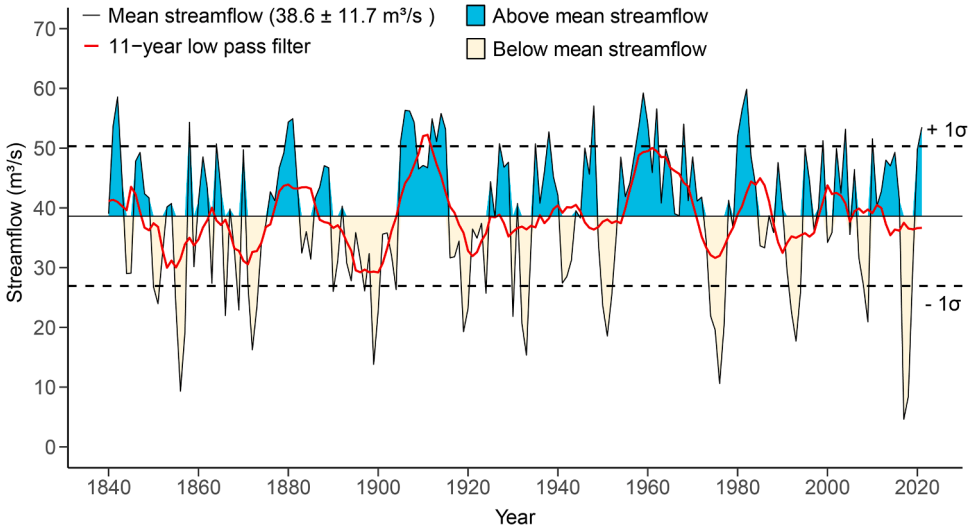


Fig. 6. Streamflow variations in the reconstructed May-June streamflow records for the Zemu River since 1840 with the upper and lower dash-lines represent high and low streamflow values above the mean +1σ and below mean − 1σ. The thick red line shows 11-year moving average streamflow.

Table 3
List of low and high streamflow years in the reconstruction.

Low flow				High flow			
Year	Streamflow (m^3/s)	Year	Streamflow (m^3/s)	Year	Streamflow (m^3/s)	Year	Streamflow (m^3/s)
1850	26.8	1930	21.9	1841	53.7	1935	50.7
1851	24.0	1932	20.6	1842	58.6	1938	52.7
1855	23.3	1933	15.4	1858	54.3	1948	57.1
1856	9.3	1950	23.6	1864	50.7	1958	53.6
1857	19.3	1951	18.6	1880	54.4	1959	59.2
1866	22.0	1952	25.5	1881	54.9	1960	54.1
1869	23.0	1974	21.9	1905	51.2	1962	56.6
1872	16.3	1975	19.6	1906	56.3	1968	54.0
1873	23.4	1976	10.6	1907	56.2	1980	52.0
1890	26.0	1977	20.4	1908	54.3	1981	56.4
1897	26.1	1992	22.5	1912	54.9	1982	59.8
1899	13.8	1993	17.7	1913	51.1	1999	51.2
1900	22.8	1994	25.9	1914	55.8	2004	53.2
1904	26.3	2009	20.9	1915	53.2	2010	51.6
1919	19.3	2017	4.6	1927	50.7	2021	53.5
1920	23.2	2018	8.5				
1924	25.7						

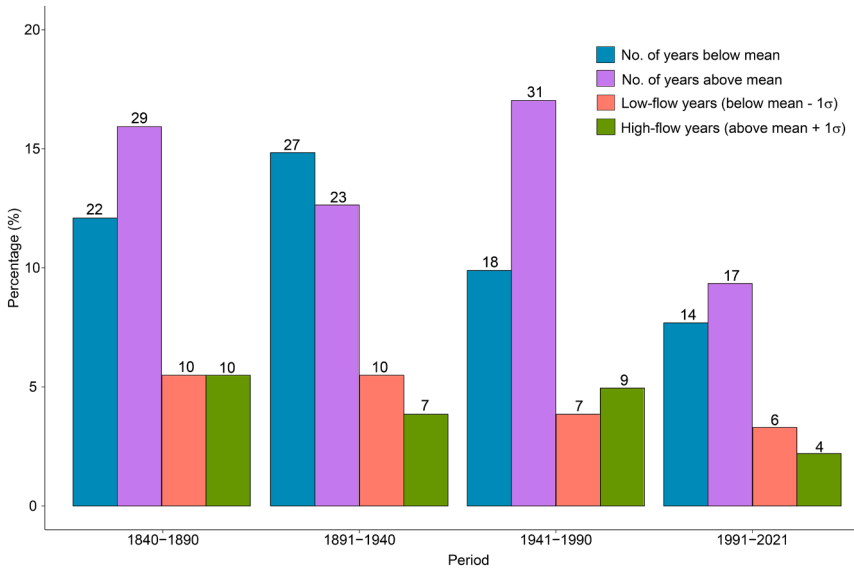


Fig. 7. Percentage of below average-flow, above average-flow, low-flow, and high-flow years in the streamflow reconstruction over 50-year windows for the period 1840–2021. Values above individual columns represent the number of years during the four different periods.

4. Discussion

In this study, the sign of the association, i.e., the significantly negative relationship between our variance stabilized ensemble chronology and Zemu River May-June streamflow is unexpected. In low-lying non-glaciated catchments in the Himalaya the association is commonly positive (Gaire et al., 2022; Shah et al., 2019, 2014) as in arid regions (Allen et al., 2024; Li et al., 2019; Woodhouse, 2001). Several other studies have found significant negative correlations between tree growth and streamflow in the glacierised catchments in the Western Himalaya (Husna et al., 2025), the Caucasus mountains (Bakhtiyorov et al., 2024), and in the Victorian Alps in Australia (O'Connor et al., 2022). This negative association likely occurs due to the dominance of glacial meltwater in driving streamflow, particularly during the growing season. In the warmer conditions, increasing meltwater leads to higher streamflow. However, at these altitudes, warmer conditions are commonly also drier such that trees may experience drought stress. Warmer conditions may also cause earlier melt of the snowpack. Both of these may reduce tree growth at the same time that there is greater ice melt, runoff and river flow. Our May-June streamflow reconstruction of the Zemu River, based on a strong and significant negative relationship between RWI chronology and observed streamflow, suggests that catchments with glaciers create different streamflow-tree growth relationships to those elsewhere. Glacierised and non-glacierised catchments should be considered differently vis-à-vis the conditions responsible for a hydrological response in tree ring proxies.

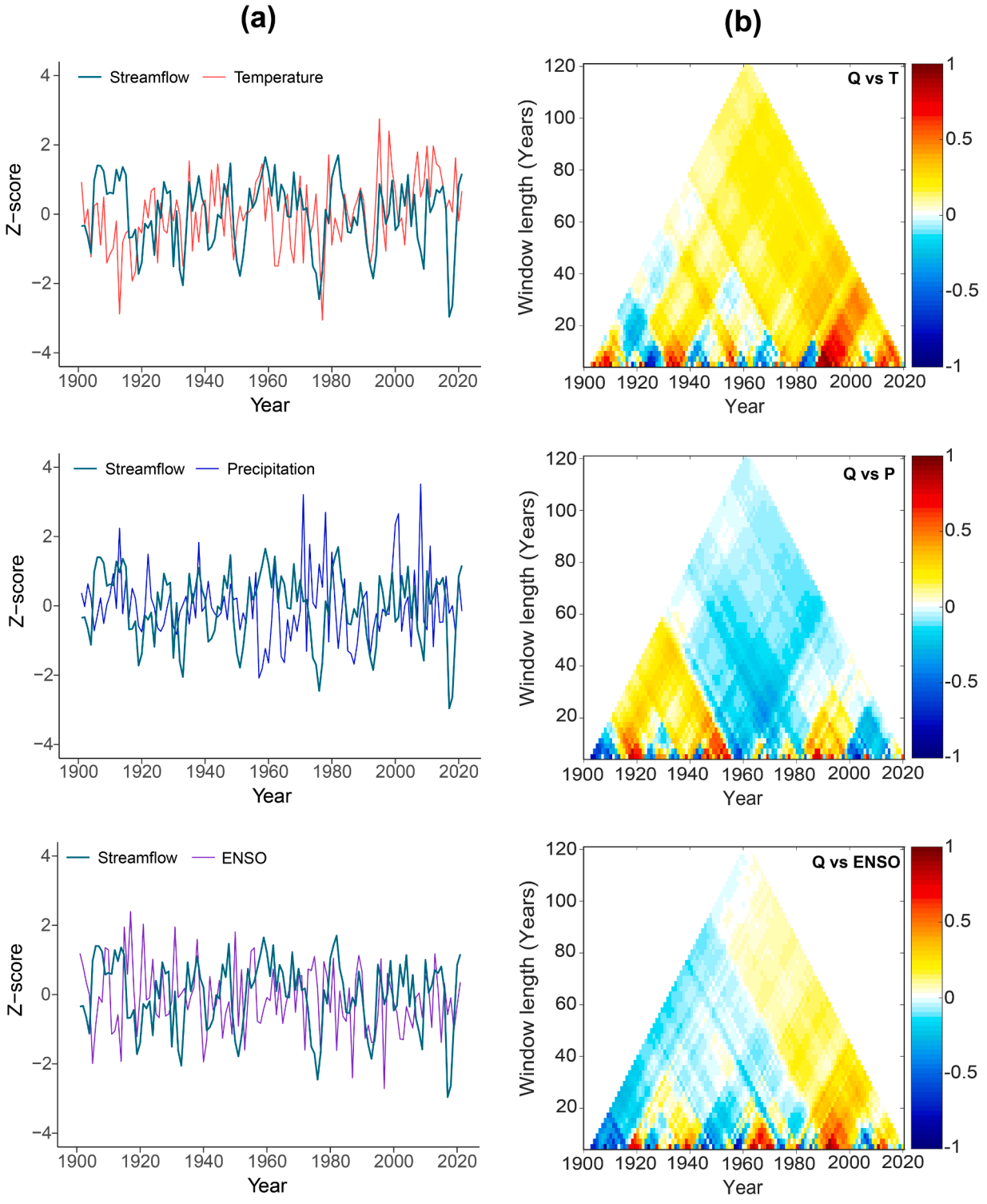


Fig. 8. Correlation (a) and Pearson window correlation (b) of reconstructed streamflow (Q) with temperature (T), precipitation (P), and ENSO. For each combination in the Pearson window correlation, the colour plot indicates the correlation strength in calendar year and varying window length.

To examine the spatial representativeness of our streamflow reconstruction, we have compared it with other streamflow reconstructions from neighbouring catchments (Fig. 9). The latter include reconstructions for the Zemu river (Chuphal and Mishra, 2023), the Lachen river (Shah et al., 2014), the Gimliang river and Lohit river (Shah et al., 2019), and the Brahmaputra river (Rao et al.,

2020). All reconstructions in Fig. 9 are based on tree-ring proxy data and instrumental streamflow records from the nearest gauges except for the study of Chuphal and Mishra (2023), which was based on the mizuRoute hydrological model (Mizukami et al., 2016). However, the streamflow reconstruction of Chuphal and Mishra (2023) shows good agreement with the others in terms of high streamflow and low streamflow periods. All the earlier studies, including ours, report low streamflow periods for 1890–1898, 1991–1995, and 2017–2019 and high streamflow periods between 1925 and 1930, 1984–1991 and 1996–2002. Compared to other streamflow reconstructions, our reconstruction shows quinquennial to decadal (i.e., 5–10 years) variabilities, and a slight pattern of shorter low-flow and high-flow periods for a number of consecutive years, e.g., low-flow between 1855 and 1857, 1974–1977, 1992–1994, and 2017–2019; and high-flow between 1912 and 1915, and 1980–1982.

Long-term hydrological conditions vary depending on the catchment characteristics and to the changes in relative contribution from different sources such as snow-, glacier-melt, precipitation and groundwater. For instance, the Zemu catchment is predominantly snow-covered with a glacier upstream, hence the Zemu River receives additional meltwater from this glacier in addition to the seasonal snowmelt and monsoon rainfall (Shah et al., 2014; Shekhar and Bhattacharyya, 2015). Unlike Zemu, the Gimliang catchment is a non-glaciated catchment with relatively less snow-cover. The Gimliang River is pre-dominantly fed by monsoon precipitation with less contribution from seasonal snow, and no glacier meltwater supply. This is most likely the reason that in-spite of similar hydrological characteristics and catchment size to the Zemu catchment, the average unit runoff in the Gimilang River (7.3 ± 2.6 mm/s) is lower than the Zemu River (9.8 ± 3.0 mm/s). On the other hand, the highest average unit runoff (26.7 ± 6.3 mm/s) was observed in the Lachen River catchment. This may be because the Lachen River has a number of upstream tributaries including the Zemu and it has a significantly larger catchment area (2080 km^2). Catchment-wise, runoff for four different 50-year periods (e.g., 1840–1890, 1891–1940, 1941–1990, and 1991–2021) were calculated together with identifying 10 most low- and high-streamflow years and the results are shown in the supplementary file S2. Results illustrate no significant trend in the long-term runoff change in these catchments. In the Zemu River average runoff appears to have varied between 50-year periods, for instance during 1840–1890 (9.6 ± 2.8 mm/s), 1891–1940 (9.7 ± 2.9 mm/s), 1941–1990 (10.3 ± 2.9 mm/s), and 1991–2021 (9.5 ± 3.3 mm/s); but these changes are negligible and there are no time-dependent trends that are significant ($p > 0.05$) based upon Mann Kendall test. These results also show that the overall runoff in this study (9.8 ± 3.0 mm/s) is higher than the runoff (5.2 ± 2.9 mm/s) modelled by Chuphal and Mishra (2023). This difference for the same catchment could be due to the use of different methods to reconstruct streamflow. We used the instrumental streamflow record from the Zemu gauge station located in the catchment; Chuphal and Mishra (2023) used observed data from a gauge located at the outlet of the Brahmaputra River. As a glacier-fed river, the streamflow of Zemu River is predominantly controlled by glacier melt, consequently monsoon precipitation may have relatively less impact as shown in Fig. 4. Thus, changes in Zemu River streamflow are more likely linked to rapid warming and glacier retreat producing higher meltwater contributions. This observation has been made for other Himalayan rivers in recent decades (Lee et al., 2021; Pritchard, 2019; Sigdel et al., 2020). A significant amount of glacier mass loss (6.8 ± 2.1 Gt) and around 797 ± 19.7 m of retreat of the Zemu glacier has been reported between 1931 and 2012 (Rashid and Majeed, 2020). An increasing rate of glacier retreat (Rashid and Majeed, 2020; Saha et al., 2024), and a gradually northward weakening of summer monsoon (Duan et al., 2006; Saini and Attada, 2023; Sano et al., 2013; Tada et al., 2016) may indicate that the glacier meltwater contribution will be the primary contributor to the streamflow in Zemu River in the future.

The warm phase of ENSO (El Niño) has traditionally been associated with a weaker ISM and the cold phase with a stronger ISM (Goswami and An, 2023; Kumar et al., 1999). Several studies have reported that ENSO has been a dominant control over the ISM rainfall since early 1900s (Aneesh and Bódai, 2024; Dwivedi et al., 2015; Goswami and An, 2023; Lin et al., 2024) and acts as a significant driver for flooding in the Himalayan Mountain and its low-lying floodplains (Gaire et al., 2022; Shah et al., 2019; Shaman et al., 2005). Other studies have suggested a weakening relationship between ENSO and ISM since the 1970s (Aneesh and Bódai, 2024; Athira et al., 2023) but it is now thought that this weakening was part of interdecadal variations (Kumar et al., 1999), and since the late 1990s the relationship has strengthened again (Yang and Huang, 2021). In a river catchment that is well into the interior Himalaya, as is the Zemu, with a very marked glacier cover, we would expect warmer and drier pre-monsoon periods (i.e., May-June) to increase ice melt and so to be associated with increased runoff. Thus, a positive (warm phase) ENSO should be associated with higher streamflow in the Zemu River. Fig. 8 shows this to be the case since the end of the 20th century with positive correlations becoming clear in both the temperature-streamflow and ENSO-streamflow relationships, and negative correlations in the precipitation-streamflow relationship. Similar positive association between ENSO and streamflow in the recent decades can also be seen in other reconstruction records in this region as shown in the supplementary figure S3. A tendency for positive correlations between ENSO and Zemu flow is also seen in the modelled results of Chuphal and Mishra (2023) from 2000s onwards (supplementary figure S3b), and for the Brahmaputra river (Rao et al., 2020) since the 1990s (supplementary figure S3f). This is the opposite of what is reported in non-glaciated catchments in the Ganges basin (Shrestha and Kostaschuk, 2005; Whitaker et al., 2001), where precipitation variability dominates runoff variability. For the Lachen river (Shah et al., 2014), and the Gimliang and Lohit rivers (Shah et al., 2019), the overall ENSO and streamflow relationships were negative from 1901–1999, except for a few years during the 1920s, 1970s and 2000s (supplementary figure S3c-e). However, if the relationship between ENSO and streamflow in neighbouring catchments has changed in recent decades, it cannot be confirmed due to the fact that the streamflow reconstruction of Lachen, Gimliang, Lohit and Brahmaputra rivers are more than two decades old. There is growing consensus that under temperature warming, multi-decadal scale changes in the strength of the ENSO-ISM teleconnection will trend towards a weaker teleconnection (Goswami and An, 2023). At the scale of multidecadal forcing, even with the length of our reconstructed streamflow record, it is a challenge to tease out more detailed relationships between streamflow and ENSO. However, changes in how ENSO modulates ISM are likely to be seen in runoff changes in glaciated basins in the Himalaya given the negative relationship between the ISM and runoff reported in this study.

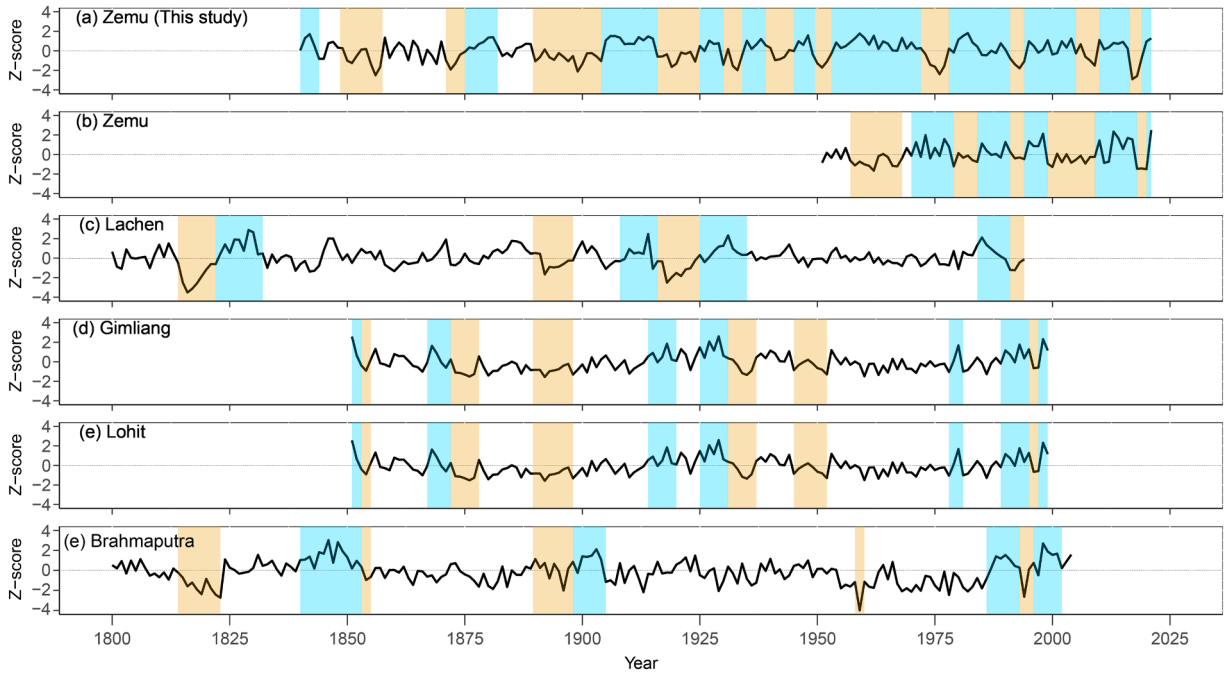


Fig. 9. Comparison between our streamflow reconstruction of the Zemu River (a) with other streamflow reconstructions including (b) the Zemu River streamflow reconstruction by Chuphal and Mishra (2023), (c) the Lachen River streamflow reconstruction (Shah et al., 2014), (d) the Gimliang River streamflow reconstruction (Shah et al., 2019), (e) the Lohit River streamflow reconstruction (Shah et al., 2019), and (f) the Brahmaputra River streamflow reconstruction (Rao et al., 2020). All reconstructed streamflow values were normalized into Z-score. The blue belt indicates high streamflow periods, and the orange belt indicates low streamflow periods.

5. Conclusions

Over recent decades, there has been increased interest in generating long-term hydrological data at ungauged or poorly gauged river basins across the Himalaya using proxy records to better understand the impacts of climate change on the Himalayan water resources. The present study has developed a tree ring chronology of *A. densa* and used it as a proxy for reconstructing pre-Monsoon (May-June) Zemu River streamflow from 1840 to 2021. The reconstruction represents only 10.7 % of the total annual streamflow during the observation period (1976–1997) but may provide useful information about hydrological conditions of Zemu river at the onset of the Indian summer monsoon. Our study shows a different streamflow response (i.e., negative correlation) as compared to other studies (i.e., positive correlations) in neighboring unglaciated sites (Shah et al., 2019, 2014). This suggests that the growth-hydroclimate relationships in glaciated catchments in mountain environments are different to non-glaciated catchments. This is because higher tree growth occurs in warmer periods that also lead to ice melt and increased runoff as compared to non-glaciated catchments where precipitation drives runoff and when temperatures are generally lower.

As indicated by our reconstruction, the Zemu River experienced five high streamflow periods (e.g., 1876–1882, 1905–1915, 1957–1962 1980–1983, and 2020–2021) and seven low streamflow periods (e.g., 1851–1857, 1866–1875, 1890–1904, 1916–1924, 1932–1934, 1973–1979, and 2017–2019) over the past 182 years. We have also identified 30 particularly high-streamflow and 33 particularly low-streamflow individual years within these periods. Windowed Pearson correlation revealed significant time-dependent responses between the reconstructed streamflow and hydroclimatic parameters at the local scale (e.g., temperature and precipitation), and other natural climate forcings such as ENSO. Our results show a positive relationship between temperature and ENSO with the reconstructed May-June streamflow in the Zemu river in recent decades. We attribute this to reduced penetration of the ISM during warm ENSO years; weakening of the ISM maintains longer warmer and drier conditions which leads to higher glacier melt contribution to the Zemu river. This explains why tree ring-based streamflow reconstructions between glaciated and non-glaciated basins show inverse responses. It also will make runoff in the Zemu and in similar rivers sensitive to the effects of global teleconnections on the strength of the ISM.

This study highlights that the variance stabilized ensemble tree-ring chronology can be useful for hydrological reconstructions in similar catchments. The Zemu catchment is mostly unexplored by humans due to its highly inaccessible terrain in the remote mountain location and this is a key appeal of the approach. However, over the recent decades, downstream of the Zemu river there has been rapid infrastructure development including roads, buildings, bridges, hydropower dams etc. This catchment may not be able to meet the increases in water demand following from such development if the number of low-flow periods continue to increase in coming years. Long-term monitoring of hydrological changes downstream can benefit from hydrological reconstruction using tree rings, but this reconstruction needs to be sensitive to how runoff-growth relations vary at the sub-catchment scale due to different glacier influence.

CRediT authorship contribution statement

Stuart N. Lane: Writing – review & editing, Validation, Supervision. **Torsten Vennemann:** Writing – review & editing, Validation, Supervision. **Nazimul Islam:** Writing – original draft, Visualization, Software, Project administration, Methodology, Investigation, Funding acquisition, Formal analysis, Data curation, Conceptualization. **Ulf Büntgen:** Writing – review & editing, Validation, Supervision. **Santosh K. Shah:** Writing – review & editing, Validation, Supervision, Data curation. **Paul J. Krusic:** Writing – review & editing, Validation, Supervision.

Declaration of Competing Interest

The authors declare the following financial interests/personal relationships which may be considered as potential competing interests Nazimul Islam reports financial support was provided by Swiss Polar Institute. Nazimul Islam reports financial support was provided by University of Lausanne. Nazimul Islam reports financial support was provided by Federal Commission for Scholarships for Foreign Students, Switzerland. If there are other authors, they declare that they have no known competing financial interests or personal relationships that could have appeared to influence the work reported in this paper.

Acknowledgements

This work was supported by the Swiss Government Excellence Scholarship (grant number: 2020.0271) of Federal Commission for Scholarships for Foreign Students (FCS), and by the Doctoral Mobility Fellowship (grant number: MD-0036) of the University of Lausanne. The Swiss Polar Institute funded the fieldwork under the Polar Access Fund (grant number PAF-2022–005). We wish to thank the officials at the Research, Evaluation and Monitoring Cell (REMC), Forest and Environment Department, Government of Sikkim and at the National Biodiversity Authority (NBA) for giving us permissions to collect tree-ring data. We are thankful to the local guides from Sikkim who were involved in data collections. We are grateful to National Hydroelectric Power Corporation (NHPC) for providing streamflow data of Zemu River and to the Climate Research Unit (CRU), University of East Anglia, UK for access to open source temperature and precipitation data. We are thankful to the laboratory technicians at the IDYST, University of Lausanne, Switzerland and at the Geography Department, University of Cambridge, UK for providing necessary facilities to prepare the data. We are equally thankful to the Swiss Federal Research Institute WSL, Switzerland for access to laboratory equipment to process the samples. Author (SKS) would like to thank, Director, BSIP, Lucknow for permission to participate in this work.

Appendix A. Supporting information

Supplementary data associated with this article can be found in the online version at doi:10.1016/j.ejrh.2025.102508.

Data availability

https://doi.org/10.5281/zenodo.15459046

References

Allen, K.J., Verdon-Kidd, D.C., Freund, M.B., Tozer, C.R., Palmer, J.G., Higgins, P.A., Saunders, K.M., Baker, P.J., 2024. Distinct geographical and seasonal signals in two tree-ring based streamflow reconstructions from Tasmania, southeastern Australia. J. Hydrol. Reg. Stud. 52, 101736. https://doi.org/10.1016/j.ejrh.2024.101736.

Aneesh, S., Bódai, T., 2024. Inter-model robustness of the forced change of the ENSO-Indian summer monsoon teleconnection. npj Clim. Atmos. Sci. 7. https://doi.org/10.1038/s41612-023-00541-w.

Athira, K.S., Roxy, M.K., Dasgupta, P., Saranya, J.S., Singh, V.K., Attada, R., 2023. Regional and temporal variability of Indian summer monsoon rainfall in relation to El Niño southern oscillation. Sci. Rep. 13. https://doi.org/10.1038/s41598-023-38730-5.

Bakhtiyorov, Z., Chen, F., Chen, Y., Wang, S., Zhang, H., Hu, M., Yue, W., Habibulloev, S., Kavtaradze, G., Gurskaya, M., Agafonov, L., Rahmonov, O., Roibu, C.C., Akkemik, U., Köse, N., Norman, C., 2024. Historical drivers and future streamflow variations of the Kura River in the Western Transcaucasia region of Georgia: analysis of tree-ring chronologies from 1720 to 2021 CE. Palaeogeogr. Palaeoclimatol. Palaeoecol. 655, 112529. https://doi.org/10.1016/j.palaeo.2024.112529.

Briffa, K.R., Jones, P.D., Bartholin, T.S., Eckstein, D., Schweingruber, F.H., Karlén, W., Zetterberg, P., Eronen, M., 1992. Fennoscandian summers from ad 500: temperature changes on short and long timescales. Clim. Dyn. 7, 111–119. https://doi.org/10.1007/BF00211153.

Briffa, K.R., Melvin, T.M., 2011. A Closer Look at Regional Curve Standardization of Tree-Ring Records: Justification of the Need, a Warning of Some Pitfalls, and Suggested Improvements in Its Application. In: Hughes, M., Swetnam, T., Diaz, H. (Eds.), Developments in Paleoenvironmental Research, Dendroclimatology. Springer, Dordrecht, pp. 113–145. https://doi.org/10.1007/978-1-4020-5725-0_5.

Bunn, A.G., 2008. A dendrochronology program library in R (dplR). Dendrochronologia 26, 115–124. https://doi.org/10.1016/j.dendro.2008.01.002.

Bunn, A.G., 2010. Statistical and visual crossdating in R using the dplR library. Dendrochronologia 28, 251–258. https://doi.org/10.1016/j.dendro.2009.12.001.

Büntgen, U., Krusic, P.J., Verstege, A., Sangüesa-Barreda, G., Wagner, S., Camarero, J.J., Ljungqvist, F.C., Zorita, E., Oppenheimer, C., Konter, O., Tegel, W., Gärtner, H., Cherubini, P., Reinig, F., Esper, A.J., 2017. New tree-ring evidence from the pyrenees reveals western mediterranean climate variability since medieval times. J. Clim. 30, 5295–5318. https://doi.org/10.1175/JCLI-D-16-0526.1.

Buras, A., 2017. A comment on the expressed population signal. Dendrochronologia 44, 130–132. https://doi.org/10.1016/j.dendro.2017.03.005.

Bussberg, N.W., Maxwell, J.T., Robeson, S.M., Huang, C., 2020. The effect of end-point adjustments on smoothing splines used for tree-ring standardization. Dendrochronologia 60, 125665. https://doi.org/10.1016/j.dendro.2020.125665.

Carrer, M., Dibona, R., Prendin, A.L., Brunetti, M., 2023. Recent waning snowpack in the Alps is unprecedented in the last six centuries. Nat. Clim. Chang 13, 155–160. https://doi.org/10.1038/s41558-022-01575-3.
Chuphal, D.S., Mishra, V., 2023. Hydrological model-based streamflow reconstruction for Indian sub-continental river basins, 1951–2021. Sci. Data 10, 1–12. https://doi.org/10.1038/s41597-023-02618-w.
Cook, E.R., 1985. A time series analysis approach to tree ring standardization [WWW Document]. Univ. Ariz. URL. ⟨https://repository.arizona.edu/handle/10150/188110⟩. accessed 4.13.20.
Cook, E.R., Briffa, K.R., Meko, D.M., Graybill, D.A., Funkhouser, G., 1995. Chronology development for palaeoclimatic studies. Holocene 5, 229–237.
Cook, E.R., Holmes, R.L., 1996. User's manual for program ARSTAN (No. program library version). Int. treering data Bank (Tucson, USA).
Cook, E.R., Krusic, P.J., L, H.R., 2017. Program ARSTAN (version 49v1a) autoregressive tree–ring standardization program [WWW Document]. TreeRing Lab. Columbia Univ. LamontDoherty Earth Obs. URL. ⟨https://www.geog.cam.ac.uk/research/projects/dendrosoftware/⟩. accessed 4.1.24.
Cook, E.R., Peters, K., 1981. The smoothing spline: a new approach to standardizing forest interior tree-ring width series for dendroclimatic studies. TreeRing Bull. 41, 45–53.
Debnath, M., Syiemlieh, H.J., Sharma, M.C., Kumar, R., Chowdhury, A., Lal, U., 2018. Glacial lake dynamics and lake surface temperature assessment along the Kangchengayo-Pauhunri Massif, Sikkim Himalaya, 1988–2014. Remote Sens. Appl. Soc. Environ. 9, 26–41. https://doi.org/10.1016/j.rsase.2017.11.002.
Dimri, A.P., Kumar, D., Choudhary, A., Maharana, P., 2018. Future changes over the Himalayas: Mean temperature. Glob. Planet. Change 162, 235–251. https://doi.org/10.1016/j.gloplacha.2018.01.014.
Douglass, A.E., 1919. Climatic cycles and tree-growth: a study of the annual rings of trees in relation to climate and solar activity. Carne Inst. Wash. https://doi.org/10.5962/bhl.title.121855.
Duan, K., Yao, T., Thompson, L.G., 2006. Response of monsoon precipitation in the Himalayas to global warming. J. Geophys. Res. Atmos. 111, 1–8. https://doi.org/10.1029/2006JD007084.
Dwivedi, S., Goswami, B.N., Kucharski, F., 2015. Unraveling the missing link of ENSO control over the Indian monsoon rainfall. Geophys. Res. Lett. 42, 8201–8207. https://doi.org/10.1002/2015GL065909.
Frank, D., Esper, J., Cook, E., 2006. On Variance Adjustments in Tree-Ring Chronology Development. In: Heinrich, I., Gärtner, H., Monbaron, M., Schleser, G. (Eds.), Tree Rings in Archaeology, Climatology and Ecology, TRACE, pp. 56–66.
Friedman, J.H., 1984. A Variable Span Smoother, Technical Report 5. Laboratory for Computational Statistics Department of Statistics. Stanford University, California.
Fritts, H.C., 1971. Dendroclimatology and dendroecology. Quat. Res. 1, 419–449. https://doi.org/10.1016/0033-5894(71)90057-3.
Fritts, H.C., 1976. Tree Rings and Climate. Academic Press INC, New York. https://doi.org/10.1016/b978-0-12-268450-0.x5001-0.
Gaire, N.P., Bhuju, D.R., Koirala, M., Shah, S.K., Carrer, M., Timilsena, R., 2017. Tree-ring based spring precipitation reconstruction in western Nepal Himalaya since AD 1840. Dendrochronologia 42, 21–30. https://doi.org/10.1016/j.dendro.2016.12.004.
Gaire, N.P., Dhakal, Y.R., Shah, S.K., Fan, Z.X., Bräuning, A., Thapa, U.K., Bhandari, S., Aryal, S., Bhuju, D.R., 2019. Drought (scPDSI) reconstruction of trans-Himalayan region of central Himalaya using Pinus wallichiana tree-rings. Palaeogeogr. Palaeoclimatol. Palaeoecol. 514, 251–264. https://doi.org/10.1016/j.palaeo.2018.10.026.
Gaire, N.P., Dhakal, Y.R., Shah, S.K., Fan, Z.-X., 2024. Potential of tree-ring chronologies for multi-centennial streamflow reconstructions: an insight from Nepal. Proc. IAHS 387, 33–39. https://doi.org/10.5194/piahs-387-33-2024.
Gaire, N.P., Zaw, Z., Bräuning, A., Sharma, B., Raj Dhakal, Y., Timilsena, R., Shah, S.K., Raj Bhuju, D., Fan, Z.X., 2022. Increasing extreme events in the central Himalaya revealed from a tree-ring based multi-century streamflow reconstruction of Karnali River Basin. J. Hydrol. 610, 127801. https://doi.org/10.1016/j.jhydrol.2022.127801.
García-López, M.A., Rozas, V., Olano, J.M., Sangüesa-Barreda, G., García-Hidalgo, M., Gómez-González, S., López-Rubio, R., Fernández-Palacios, J.M., García-González, I., García-Cervigón, A.I., 2022. Tree-ring distinctness, dating potential and climatic sensitivity of laurel forest tree species in Tenerife Island. Dendrochronologia 76. https://doi.org/10.1016/j.dendro.2022.126011.
Gärtner, H., Schneider, L., Cherubini, P., 2024. A New Workflow for Sampling and Digitizing Increment Cores. J. Vis. Exp., e67098 https://doi.org/10.3791/67098.
Goswami, B.B., An, S.-I., 2023. An assessment of the ENSO-monsoon teleconnection in a warming climate. npj Clim. Atmos. Sci. 6. https://doi.org/10.1038/s41612-023-00411-5.
Gou, X.H., Deng, Y., Chen, F.H., Yang, M.X., Fang, K.Y., Gao, L.L., Yang, T., Zhang, F., 2010. Tree ring based streamflow reconstruction for the Upper Yellow River over the past 1234 years. Chin. Sci. Bull. 55, 4179–4186. https://doi.org/10.1007/s11434-010-4215-z.
Grissino-Mayer, H., 2001. Evaluating Crossdating Accuracy: A Manual and Tutorial for the Computer Program COFECHA. Tree-ring Res.
Harris, I., Osborn, T.J., Jones, P., Lister, D., 2020. Version 4 of the CRU TS monthly high-resolution gridded multivariate climate dataset. Sci. Data 7, 1–18. https://doi.org/10.1038/s41597-020-0453-3.
Helama, S., Melvin, T.M., Briffa, K.R., 2017. Regional curve standardization: State of the art. Holocene 27, 172–177. https://doi.org/10.1177/0959683616652709.
Holmes, R., 1983. Computer-Assisted Quality Control in Tree-Ring Dating and Measurement. Treering Bull. 43, 69–78.
Huber, P.J., 1981. Robust statistics. Wiley, New York, USA.
Husna, A., Shah, S.K., Mehrotra, N., Thomte, L., Rahman, T.W., Pandey, U., Islam, N., Gaire, N.P., Singh, D., 2025. Streamflow Reconstruction Using Multi-Taxa Tree-Ring Records from Kullu Valley, Himachal Pradesh, Western Himalaya. Quaternary 8, 9. https://doi.org/10.3390/quat8010009.
Immerzeel, W.W., Lutz, A.F., Andrade, M., Bahl, A., Biemans, H., Bolch, T., Hyde, S., Brumby, S., Davies, B.J., Elmore, A.C., Emmer, A., Feng, M., Fernández, A., Haritashya, U., Kargel, J.S., Koppes, M., Kraaijenbrink, P.D.A., Kulkarni, A.V., Mayewski, P.A., Nepal, S., Pacheco, P., Painter, T.H., Pellicciotti, F., Rajaram, H., Rupper, S., Sinisalo, A., Shrestha, A.B., Viviroli, D., Wada, Y., Xiao, C., Yao, T., Baillie, J.E.M., 2020. Importance and vulnerability of the world's water towers. Nature 577, 364–369. https://doi.org/10.1038/s41586-019-1822-y.
Immerzeel, W.W., Van Beek, L.P.H., Bierkens, M.F.P., 2010. Climate change will affect the asian water towers. Science 328, 1382–1385. https://doi.org/10.1126/science.1183188.
Islam, N., Patel, P.P., 2021. Inventory and GLOF hazard assessment of glacial Lakes in the Sikkim Himalayas, India. Geocarto Int. 37, 3840–3876. https://doi.org/10.1080/10106049.2020.1869332.
Islam, N., Vennemann, T., Büntgen, U., Cherubini, P., Lane, S.N., 2024. Tree-ring hydrological research in the Himalaya: state of the art and future directions. Prog. Phys. Geogr. https://doi.org/10.1177/03091333241229919.
Jaffrés, J.B.D., 2019. GHCN-Daily: a treasure trove of climate data awaiting discovery. Comput. Geosci. 122, 35–44. https://doi.org/10.1016/j.cageo.2018.07.003.
Jevšenak, J., Levanič, T., 2018. dendroTools: R package for studying linear and nonlinear responses between tree-rings and daily environmental data. Dendrochronologia 48, 32–39. https://doi.org/10.1016/j.dendro.2018.01.005.
Kääb, A., Berthier, E., Nuth, C., Gardelle, J., Arnaud, Y., 2012. Contrasting patterns of early twenty-first-century glacier mass change in the Himalayas. Nature 488, 495–498. https://doi.org/10.1038/nature11324.
Katel, O.N., Schmidt-Vogt, D., Dendup, N., 2015. Transboundary Water Resources Management in the Context of Global Environmental Change: The Case of Bhutan Himalaya. In: Shrestha, S., Anal, A.K., Salam, P.A., Van Der Valk, M. (Eds.), Managing Water Resources Under Climate Uncertainty: Examples from Asia, Europe, Latin America, and Australia. Springer, Cham, pp. 269–290. https://doi.org/10.1007/978-3-319-10467-6_13.
Kattel, G.R., Paszkowski, A., Pokhrel, Y., Wu, W., Li, D., Rao, M.P., 2023. How resilient are waterways of the Asian Himalayas? Finding adaptive measures for future sustainability. Wiley Interdiscip. Rev. Water 10, 1–23. https://doi.org/10.1002/wat2.1677.
Kayastha, R.B., Kayastha, R., 2019. Glacio-hydrological degree-day model (gdm) useful for the himalayan river basins. Himal. Weather Clim. Their Impact Environ. 379–398. https://doi.org/10.1007/978-3-030-29684-1_19.
Kraaijenbrink, P.D.A., Bierkens, M.F.P., Lutz, A.F., Immerzeel, W.W., 2017. Impact of a global temperature rise of 1.5 degrees Celsius on Asia's glaciers. Nature 549, 257–260. https://doi.org/10.1038/nature23878.

Kumar, K.K., Rajagopalan, B., Cane, M.A., 1999. On the weakening relationship between the indian monsoon and ENSO. Science 284, 2156–2159. https://doi.org/10.1126/science.284.5423.2156.
Lee, E., Carrivick, J.L., Quincey, D.J., Cook, S.J., James, W.H.M., Brown, L.E., 2021. Accelerated mass loss of Himalayan glaciers since the Little Ice Age. Sci. Rep. 11, 24284. https://doi.org/10.1038/s41598-021-03805-8.
Li, D., Lu, X., Overeem, I., Walling, D.E., Syvitski, J., Kettner, A.J., Bookhagen, B., Zhou, Y., Zhang, T., 2021. Exceptional increases in fluvial sediment fluxes in a warmer and wetter High Mountain Asia. Science (80.) 374, 599–603. https://doi.org/10.1126/science.abi9649.
Li, J., Wang, Z., Lai, C., Zhang, Z., 2019. Tree-ring-width based streamflow reconstruction based on the random forest algorithm for the source region of the Yangtze River, China. Catena 183, 104216. https://doi.org/10.1016/j.catena.2019.104216.
Lin, S., Dong, B., Yang, S., Zhang, T., 2024. Diverse impacts of the Indian summer monsoon on ENSO among CMIP6 models and its possible causes. Environ. Res. Lett. 19. https://doi.org/10.1088/1748-9326/ad6618.
Matheus, T.J., 2014. A 332-year reconstruction of midwest droughts from tree-rings. Indiana University, USA. https://doi.org/10.13140/RG.2.2.14680.19205.
Maxwell, R.S., Larsson, L.A., 2021. Measuring tree-ring widths using the CooRecorder software application. Dendrochronologia 67, 125841. https://doi.org/10.1016/j.dendro.2021.125841.
Melvin, T.M., Briffa, K.R., Nicolussi, K., Grabner, M., 2007. Time-varying-response smoothing. Dendrochronologia 25, 65–69. https://doi.org/10.1016/j.dendro.2007.01.004.
Michaelsen, J., 1987. Cross-validation in statistical climate forecast models. J. Clim. Appl. Meteor. 26, 1589–1600. https://doi.org/10.1175/1520-0450(1987)026%3C1589:CVISCF%3E2.0.CO;2.
Mizukami, N., Clark, M.P., Sampson, K., Nijssen, B., Mao, Y., McMillan, H., Viger, R.J., Markstrom, S.L., Hay, L.E., Woods, R., Arnold, J.R., Brekke, L.D., 2016. MizuRoute version 1: a river network routing tool for a continental domain water resources applications. Geosci. Model Dev. 9, 2223–2228. https://doi.org/10.5194/gmd-9-2223-2016.
O'Connor, J.A., Henley, B.J., Brookhouse, M.T., Allen, K.J., 2022. Ring-width and blue-light chronologies of Podocarpus lawrencei from southeastern mainland Australia reveal a regional climate signal. Clim 18, 2567–2581. https://doi.org/10.5194/cp-18-2567-2022.
Osborn, T.J., Briffa, K.R., Jones, P.D., 1997. Adjusting variance for sample-size in tree-ring chronologies and other regional mean timeseries. Dendrochronologia 15, 89–99.
Pepin, N.C., Arnone, E., Gobiet, A., Haslinger, K., Kotlarski, S., Notarnicola, C., Palazzi, E., Seibert, P., Serafin, S., Schöner, W., Terzago, S., Thornton, J.M., Vuille, M., Adler, C., 2022. Climate changes and their elevational patterns in the mountains of the world. Rev. Geophys 60, 1–40. https://doi.org/10.1029/2020RG000730.
Pepin, N., Bradley, R.S., Diaz, H.F., Baraer, M., Caceres, E.B., Forsythe, N., Fowler, H., Greenwood, G., Hashmi, M.Z., Liu, X.D., Miller, J.R., Ning, L., Ohmura, A., Palazzi, E., Rangwala, I., Schöner, W., Severskiy, I., Shahgedanova, M., Wang, M.B., Williamson, S.N., Yang, D.Q., 2015. Elevation-dependent warming in mountain regions of the world. Nat. Clim. Chang 5, 424–430. https://doi.org/10.1038/nclimate2563.
Pritchard, H.D., 2019. Asia's shrinking glaciers protect large populations from drought stress. Nature 569, 649–654. https://doi.org/10.1038/s41586-019-1240-1.
Rangwala, I., Miller, J.R., 2012. Climate change in mountains: a review of elevation-dependent warming and its possible causes. Clim. Change 114, 527–547. https://doi.org/10.1007/s10584-012-0419-3.
Rani, Seema, Kumar, Rajesh, Maharana, P., 2022. Climate Change, Its Impacts, and Sustainability Issues in the Indian Himalaya: An Introduction. In: Rani, S., Kumar, R. (Eds.), Climate Change. Springer, Cham, pp. 1–27. https://doi.org/10.1007/978-3-030-92782-0_1.
Rao, M.P., Cook, E.R., Cook, B.I., D'Arrigo, R.D., Palmer, J.G., Lall, U., Woodhouse, C.A., Buckley, B.M., Uriarte, M., Bishop, D.A., Jian, J., Webster, P.J., 2020. Seven centuries of reconstructed Brahmaputra River discharge demonstrate underestimated high discharge and flood hazard frequency. Nat. Commun. 11, 6017. https://doi.org/10.1038/s41467-020-19795-6.
Rashid, I., Majeed, U., 2020. Retreat and geodetic mass changes of Zemu Glacier, Sikkim Himalaya, India, between 1931 and 2018. Reg. Environ. Chang 125.
Reinsch, C.H., 1967. Smoothing by spline functions. Numer. Math. 10, 177–183.
Reinsch, C.H., 1971. Smoothing by spline functions II. Numer. Math. 16, 451–454. https://doi.org/10.1007/BF02169154.
Roe, G.H., Baker, M.B., Herla, F., 2017. Centennial glacier retreat as categorical evidence of regional climate change. Nat. Geosci. 10, 95–99. https://doi.org/10.1038/ngeo2863.
Ropelewski, C.F., Jones, P.D., 1987. An extension of the Tahiti-Darwin Southern Oscillation Index. Mon. Weather Rev. 115, 2161–2165. https://doi.org/10.1175/1520-0493(1987)115%3C2161:AEOTTS%3E2.0.CO;2.
Rousseeuw, P.J., Leroy, A.M., 1987. Robust regression and outlier detection. Wiley, New York, USA.
Saha, S., Bera, B., Bhattacharjee, S., Sengupta, N., Barman, M., 2024. Significant changes of area, length and terminus of Sikkim Himalayan glaciers within the Kanchenjunga national park from 1990 - 2022. Results Earth Sci. 2, 100013. https://doi.org/10.1016/j.rines.2023.100013.
Saini, R., Attada, R., 2023. Analysis of Himalayan summer monsoon rainfall characteristics using Indian High-Resolution Regional Reanalysis. Int. J. Clim. 43, 4286–4307. https://doi.org/10.1002/joc.8087.
Sano, M., Tshering, P., Komori, J., Fujita, K., Xu, C., Nakatsuka, T., 2013. May-September precipitation in the Bhutan Himalaya since 1743 as reconstructed from tree ring cellulose δ18O. J. Geophys. Res. Atmos. 118, 8399–8410. https://doi.org/10.1002/jgrd.50664.
Schmeller, D.S., Urbach, D., Bates, K., Catalan, J., Cogălniceanu, D., Fisher, M.C., Friesen, J., Füreder, L., Gaube, V., Haver, M., Jacobsen, D., Le Roux, G., Lin, Y.P., Loyau, A., Machate, O., Mayer, A., Palomo, I., Plutzar, C., Sentenac, H., Sommaruga, R., Tiberti, R., Ripple, W.J., 2022. Scientists' warning of threats to mountains. Sci. Total Environ. 853. https://doi.org/10.1016/j.scitotenv.2022.158611.
Schulman, E., 1956. Dendroclimatic Changes in Semiarid America. University of Arizona Press, Tucson, AZ, USA.
Shah, S.K., Bhattacharyya, A., Chaudhary, V., 2014. Streamflow reconstruction of Eastern Himalaya River, Lachen "Chhu", North Sikkim, based on tree-ring data of Larix griffithiana from Zemu Glacier basin. Dendrochronologia 32, 97–106. https://doi.org/10.1016/j.dendro.2014.01.005.
Shah, S.K., Singh, R., Mehrotra, N., Thomte, L., 2019. River flow reconstruction of the Lohit River Basin, North-east India based on tree-rings of Pinus merkusii (Merkus pine). J. Palaeosci. 68, 113–124. https://doi.org/10.54991/jop.2019.38.
Shaman, J., Cane, M., Kaplan, A., 2005. The relationship between tibetan snow depth, ENSO, river discharge and the monsoons of Bangladesh. Int. J. Remote Sens 26, 3735–3748. https://doi.org/10.1080/01431160500185599.
Shekhar, M., Bhattacharyya, A., 2015. Reconstruction of January-April discharge of Zemu Chuu - A first stage of Teesta River North Sikkim Eastern Himalaya based on tree-ring data of fir. J. Hydrol. Reg. Stud. 4, 776–786. https://doi.org/10.1016/j.ejrh.2015.06.019.
Shrestha, A., Kostaschuk, R., 2005. El Niño/Southern Oscillation (ENSO)-related variablity in mean-monthly streamflow in Nepal. J. Hydrol. 308, 33–49. https://doi.org/10.1016/j.jhydrol.2004.10.020.
Shrestha, F., Steiner, J.F., Shrestha, R., Dhungel, Y., Joshi, S.P., Inglis, S., Ashraf, A., Wali, S., Walizada, K.M., Zhang, T., 2023. A comprehensive and version-controlled database of glacial lake outburst floods in High Mountain Asia. Earth Syst. Sci. Data 15, 3941–3961. https://doi.org/10.5194/essd-15-3941-2023.
Shukla, A., Garg, P.K., Srivastava, S., 2018. Evolution of glacial and high-altitude lakes in the Sikkim, Eastern Himalaya over the past four decades (1975-2017). Front. Environ. Sci. 6, 1–19. https://doi.org/10.3389/fenvs.2018.00081.
Sigdel, S.R., Zhang, H., Zhu, H., 2020. Retreating Glacier and Advancing Forest Over the Past 200 Years in the Central Himalayas. JGR Biogeosci. 125, e2020JG005751. https://doi.org/10.1029/2020JG005751.
Speer, J.H., 2010. Fundamentals of Tree-Ring Research. University of Arizona Press, Tucson, AZ.
Tada, R., Zheng, H., Clift, P.D., 2016. Evolution and variability of the Asian monsoon and its potential linkage with uplift of the Himalaya and Tibetan Plateau. Prog. Earth Planet. Sci. 3. https://doi.org/10.1186/s40645-016-0080-y.
Taylor, C., Robinson, T.R., Dunning, S., Rachel Carr, J., Westoby, M., 2023. Glacial lake outburst floods threaten millions globally. Nat. Commun. 14, 487. https://doi.org/10.1038/s41467-023-36033-x.
Viviroli, D., Dürr, H.H., Messerli, B., Meybeck, M., Weingartner, R., 2007. Mountains of the world, water towers for humanity: typology, mapping, and global significance. Water Resour. Res. 43, 1–13. https://doi.org/10.1029/2006WR005653.

Whitaker, D.W., Wasimi, S.A., Islam, S., 2001. The El Niño-Southern oscillation and long-range forecasting of flows in the ganges. Int. J. Clim. 21, 77–87. https://doi.org/10.1002/joc.583.

Wigley, T.M.L., Briffa, K.R., Jones, P.D., 1984. On the Average Value of Correlated Time Series, with Applications in Dendroclimatology and Hydrometeorology. J. Appl. Meteorol. Climatol. 23, 201–2013. https://doi.org/10.1175/1520-0450(1984)023%3C0201:OTAVOC%3E2.0.CO;2.

Wijngaard, R.R., Biemans, H., Lutz, A.F., Shrestha, A.B., Wester, P., Immerzeel, W.W., 2018. Climate change vs. socio-economic development: understanding the future South Asian water gap. Hydrol. Earth Syst. Sci. 22, 6297–6321. https://doi.org/10.5194/hess-22-6297-2018.

Wilson, R., Wilson, D., Rydval, M., Crone, A., Büntgen, U., Clark, S., Ehmer, J., Forbes, E., Fuentes, M., Gunnarson, B.E., Linderholm, H.W., Nicolussi, K., Wood, C., Mills, C., 2017. Facilitating tree-ring dating of historic conifer timbers using Blue Intensity. J. Archaeol. Sci. 78, 99–111. https://doi.org/10.1016/j.jas.2016.11.011.

Woodhouse, C.A., 2001. A tree-ring reconstruction of streamflow for the Colorado Front Range. J. Am. Water Resour. Assoc. 37, 561–569. https://doi.org/10.1111/j.1752-1688.2001.tb05493.x.

Yadav, R.R., 2011. Long-term hydroclimatic variability in monsoon shadow zone of western Himalaya, India. Clim. Dyn. 36, 1453–1462. https://doi.org/10.1007/s00382-010-0800-8.

Yadav, R.R., Misra, K.G., Kotlia, B.S., Upreti, N., 2014. Premonsoon precipitation variability in Kumaon Himalaya, India over a perspective of 300 years. Quat. Int. 325, 213–219. https://doi.org/10.1016/j.quaint.2013.09.005.

Yang, X., Huang, P., 2021. Restored relationship between ENSO and Indian summer monsoon rainfall around 1999/2000. Innovation 2. https://doi.org/10.1016/j.xinn.2021.100102.

Zhang, G., Bolch, T., Yao, T., Rounce, D.R., Chen, W., Veh, G., King, O., Allen, S.K., Wang, M., Wang, W., 2023. Underestimated mass loss from lake-terminating glaciers in the greater Himalaya. Nat. Geosci. 16, 333–338. https://doi.org/10.1038/s41561-023-01150-1.

Zhao, X., Zhang, R., Chen, F., Maisupova, B., Kirillov, V., Mambetov, B., Yu, S., He, Q., Dosmanbetov, D., Kelgenbayev, N., 2022. Reconstructed summertime (June–July) streamflow dating back to 1788 CE in the Kazakh Uplands as inferred from tree rings. J. Hydrol. Reg. Stud. 40. https://doi.org/10.1016/j.ejrh.2022.101007.